Conversion of sugar diacetyls to bio-hydrocarbons by the catalytic cracking in a fixed bed with fresh and deactivated Beta zeolite

Catalysis Communications 171 (2022) 106519

Contents lists available at ScienceDirect

Catalysis Communications

journal homepage: www.elsevier.com/locate/catcom

Conversion of sugar diacetyls to bio-hydrocarbons by the catalytic cracking in a fixed bed with fresh and deactivated Beta zeolite

Cristiane Cardoso [a,*], Yiu Lau Lam [a], Rosane A.S. San Gil [a], Jeroen A. Van Bokhoven [b], Marcelo Maciel Pereira [a,*]

[a] Universidade Federal do Rio de Janeiro, Instituto de Química, Rio de Janeiro, Brazil
[b] Paul Scherrer Institute, Villigen, Switzerland and Institute of Chemical and Bioengineering, ETH Zurich, Zurich, Switzerland

ARTICLE INFO

Keywords:
Bio-hydrocarbons
Sugar acetals
Biomass
Fixed bed
Zeolite

ABSTRACT

The conversion of biomass into fuel under typical refinery conditions is a promising solution to decrease carbon footprint. Herein we convert a representative compound of a new bio-petroleum, DX (1,2:3,5-di-*O*-isopropylidene-α-D-xylofuranose) mixture with n-hexane. Firstly fresh zeolites (Beta, ZSM-5 and USY) were explored. Beta zeolite showed a high performance in converting DX into hydrocarbons. Thus it was further modified by hydrothermal deactivation. This treatment reduced the acid site density of Beta, resulting in an improvement in aromatics, reducing gas 2-fold and coke 1-fold, and only leaving a small amount of oxygenates in the liquid fraction in the test with 20% DX.

1. Introduction

The increase in the world population together with continued economic growth and reliance on fossil-based fuels as primary energy sources will have important negative impacts in the future. Using second-generation biomass is an alternative to reduce the dependence on oil and shorten the path to sustainability.

Second-generation biomass is also known as lignocellulosic biomass. It is typically derived from waste such as sugarcane bagasse, so there is no competition between fuel and food. The bagasse is mainly composed of cellulose (30–50 wt%), hemicellulose (15–35 wt%) and lignin (10–50 wt%). It has a low density (~ 0.1 g.cm^{-3}) and can undergo degradation under ambient conditions [1]. Sugarcane bagasse when subjected to specific conversion processes generates a high density bio-oil (~1.1 g.cm^{-3}) [2]. This bio-oil is still a mixture of biopolymers which contains a large number of carbon-oxygen bonds, making it highly reactive [1]. On the other hand, mineral oil-derived feeds do not contain oxygen in their structure but contain different types of carbon-carbon and carbon-hydrogen bonds, which are much less reactive [3] and need high reaction temperatures and tailor-made catalysts to be converted into fuels.

So far, the bio-oil derived from pyrolysis of biomass is the main process described in the literature. For fuel production, frequently it is submitted to a fluidized catalytic cracking process (FCC) [4–6]. Nevertheless, bio-oil from pyrolysis has disadvantages [7–10], such as high acidity and viscosity, low stability and immiscibility with hydrocarbons. These characteristics make its use for fuel production unfeasible without pre-treatment [11,12]. Furthermore, the pyrolysis bio-oil is limited to 10–20% by weight in co-processing with vacuum gas oil in FCC, since a greater amount of this bio-oil results in undesirably high amounts of coke and oxygen compounds [4,13]. Hence, the drawback related to the transport of this bio-feed can be solved by increasing the density of the bio-oil compared to sugarcane bagasse fibers, but the problems related to stability and adequate reactivity for the use in the usual FCC processes still need to be resolved.

In this respect, Pereira et al. introduced the transformation of sugarcane bagasse into a bio-petroleum (BP), composed of acetyl derivatives of carbohydrates, through the protection of oxygenated groups by the acetalization reaction to produce renewable fuels [7]. The main advantages of this biofuel are low acidity, high solubility in organic solvents, adequate density, thermal stability, and the absence of sulfur and nitrogen, unlike in mineral oil products [13]. These features indicate the possibility of introducing biofuels in the feed stream of the FCC process in a co-processing arrangement, yielding mono-aromatics and saturated hydrocarbons without the need for major adaptations to the current parameters of refineries to obtain fuels [7,14,15].

An important component of bio-petroleum, 1,2-3,5-*O*-di-isopropylidene-D-xylofuranose (DX), has been used as a model to test the catalytic cracking reaction (in fixed and fluidized beds) using ZSM-5 and

* Corresponding authors.
E-mail addresses: cristianesouza@iq.ufrj.br (C. Cardoso), maciel@iq.ufrj.br (M.M. Pereira).

https://doi.org/10.1016/j.catcom.2022.106519
Received 4 August 2022; Received in revised form 15 September 2022; Accepted 26 September 2022
Available online 27 September 2022

USY catalysts [14,16]. A co-reagent, n-hexane, has been used, since it is a low-activity hydrocarbon [17–20], miscible and less reactive than DX. DX contains carbon-oxygen bonds, which are more reactive than the σC-C and σC-H bonds of n-hexane. This fact favors DX in the competition for active sites of the zeolite. Therefore, DX is able to produce a larger range of products compared to n-hexane [2].

Table 1 presents three relevant zeolites and the main characteristics for both hydrocarbon and DX cracking. The differences in product distribution originate from the zeolite properties. For instance, when converted in the presence of ZSM-5, both n-hexane and DX produce more gas and aromatics and less polyaromatics and coke due to the smaller pore in comparison with USY [17].

USY zeolite is one of the main components of FCC catalysts, responsible for the activity and selectivity in the catalytic cracking reactions [22]. USY converts large hydrocarbons (≈20 carbon chain) [23], but its large pores and high acid density favor coke formation. Thus, the coke yield can increase in converting molecules more reactive than those in vacuum gasoil (VGO). Bio-petroleum comprises large molecules, with 8 to 20 or more carbons [1]. The pores of ZSM-5 may be too small to convert the largest molecules in BP. Thus, there are drawbacks of using both ZSM-5 and USY for BP conversion.

Beta zeolite is a promising catalyst for the FCC process with bio-feeds due to its textural characteristics and acidity between zeolite USY and ZSM-5. The study of the properties of zeolite in the catalytic cracking of DX is new and of great interest, since it can help put the refining and petrochemical industry at the forefront of sustainability.

We used Beta zeolite with and without further steam treatment to convert DX mixed with n-hexane in a fixed bed reactor. We first compare fresh Beta with results from the literature of ZSM-5 and USY zeolites. Further, Beta was treated with water vapor in the range 600 °C–800 °C. This treatment has the aim of decreasing the number of active sites on the Beta zeolite. This preparation will reduce the activity of the zeolite yet may improve the product distribution from DX, particularly by reducing coke and light gas. Furthermore, it will also minimize the conversion of nC_6 in the mixture, increasing the content of the products from DX. The tests were compared with pure n-hexane as reference molecule.

2. Experimental

2.1. Preparation of catalysts

Beta zeolite (SiO_2/Al_2O_3 molar ratio 28, code CP-814E) was purchased from Zeolyst International Inc. (USA). It was calcined at 550 °C for 3 h and called HBEA. The hydrothermal treatment was carried out in a muffle furnace. It was heated from room temperature with a heating ramp of 10 °C / min to 600 °C, 720 °C, and 800 °C and was kept at this final temperature for 2 h. At this temperature, 100% steam was introduced through a deionized water evaporator at a volumetric flow rate of 1 mL / min. The samples obtained were named DHBEA600, DHBEA720, and DHBEA800 respectively.

Table 1
Characteristics of zeolites when added to a FCC catalyst for hydrocarbon and DX processing.

Zeolite	Characteristics of typical hydrocarbon cracking	Observed properties of DX cracking
ZSM-5[a] (~ 5,7 Å)	• Maximizes light olefins [17] • Does not increase coke [18] • Improves the octane level, yet lowers gasoline yields	• Increases propylene, butene and ethene selectivity [17] • Lowers loss of product in coke • Reduces polyaromatic compounds
BETA[a] (~7,3 Å)	• Improves light olefin formation but may increase coke • Increases compounds in the gasoline range [19]	• Not tested in the literature
Y[a] (~7,4 Å)	• Increases compounds in the gasoline range • Increases loss of product in coke [21]	• Increased the methane and decreased propane selectivity • Greater loss of product in coke • Increase of polyaromatics compounds [21]

[a] http://Europe.iza-structure.org images.

2.2. Catalyst characterization

The crystallinity of all catalysts was determined by X-ray diffraction (XRD) using a Rigaku Ultima IV diffractometer (Cu Kαλ = 0.1542 nm), fixed energy source (40 kV and 20 mA) and a scanning rate of 0.02° s^{-1} at 2θ intervals from 5° to 80°. The crystallographic records were obtained using the Rigaku PDXL program. Crystallinity of Beta zeolite was calculated integrating the area of the diffractograms between 7.8° and 22.4°, and normalising this value with respect to a reference sample (HBEA), which was considered to have 100% crystallinity. (Eq. S5 in the supplementary information).

The textural properties were measured with nitrogen physisorption performed at −196 °C in a Micromeritics ASAP 2420 device. Before analysis, the samples were dried at 300 °C under vacuum for 15 h and then pre-treated in-situ under vacuum at 150 °C for 1 h until reaching a maximum rate of 5μmHg min^{-1}. Specific surface area (S_{BET}) and external specific area (S_{ext}) were calculated through Brunauer-Emmett-Teller (BET) plots and t-plots, respectively. Total pore volume was determined at $0.98P/P_o$ and micropore volume was determined from the t-plots.

The catalysts' morphology was analyzed by scanning electron microscopy (SEM) with a Zeiss Gemini 1530 microscope at an acceleration voltage of 5 keV.

Catalyst acidity was measured by FTIR spectroscopy of adsorbed probe molecules, e.g., pyridine using a Thermo Nicolet iS50 FTIR spectrometer equipped with a DTGS detector at a 4 cm^{-1} optical resolution and 128 scans. Prior to the measurements, the sample (20 mg) was pressed into self-supporting discs and activated in the IR cell attached to a vacuum line at 450 °C for 2 h. The sample was cooled in vacuum to 150 °C for pyridine adsorption. After adsorption for 30 min, the excess probe molecules were evacuated at 100 °C for 0.5 h. The Py band at 1548 cm^{-1} was used for quantitative analysis assuming the extinction coefficient ε (1545 cm^{-1}) = 1.54 cm.μmol^{-1}. Difference spectra were obtained by subtracting the spectra of the reference samples from the spectra of samples with the adsorbate. For spectra data processing, the OMNIC 9.1 software was used.

The chemical compositions were determined in a Supermini 200 X-ray fluorescence spectrometer (Rigaku). Detection was performed by PC and SC detectors with an element detection range from F to U. The X-ray source consisted of a Pd lamp set at 50 kV and 4.0 mA. The powder samples were dispersed evenly in the sample holder and then analyzed in the equipment.

Solid state NMR spectra were acquired at magnetic field of 9.4 T (Bruker Avance III400WB spectrometer) at Larmor frequencies of 79.46 Mz (^{29}Si Larmor frequency) and 104.23 MHz (^{27}Al Larmor frequency). Setup and pulse calibrations were established with solid kaolinite (^{29}Si signal at −91.5 ppm) and liquid 1 M $AlCl_3.6H_2O$ (^{27}Al signal at 0.0 ppm). Solid $AlCl_3$ was used for calibration of the central transition excitation, using a factor less than 90/(I + 1/2). Acquisition details were: ^{29}Si – Bruker 7 mm HX MAS probe, spinning frequency of 3 kHz, pi/2 (8.38 microsec) pulse sequence, recycle delay of 60 s and 256 scans; and ^{27}Al – Bruker HXY triple channel 4 mm MAS probe, spinning frequency of 12 kHz, one pi/12 (1.29 microsec) pulse sequence, recycle delay of 0.5 s and 8192 scans. Quantification of framework and extra-framework Al was performed by ^{27}Al solid state MAS NMR spectra, through the measurement of relative areas (Topspin program) in the following regions: 100 to 40 ppm, framework Al; 40 to 10 ppm, distorted Al^{IV} and/or Al^{V} extra-framework Al; and 10 to −50 ppm, Al^{VI} extra-framework Al. The spectra were also simulated by employing central

transition MAS model with DMfit program, and the results showed the same trend of the integrals measured with Topspin Program.

2.3. Synthesis of DX

The 1,2:3,5-di-*O*-isopropylidene-α-D-xylofuranose (DX) was synthesized by the reaction of D-xylose (98.5%, Vetec,30 g) with acetone (99%, Vetec, 800 mL). The reactant mixture was magnetically stirred and cooled by ice bath to 10 °C. 20 mL of H_2SO_4 (98% purity, P.A., Vetec) was added dropwise to the cooled suspension for 15 min and then the system was heated to 20 °C under magnetic stirring for 90 min. The mixture was cooled to 10 °C and neutralized through dropwise addition of 80 mL of a NaOH (40 wt%) aqueous solution. The resulting suspension was filtered under vacuum and the filtrate was inserted in a rotary evaporator to evaporate acetone under low pressure at 55 °C. This step yielded a white emulsion residue, which was mixed with 120 mL of ethyl acetate, thus forming two phases. The aqueous phase was separated, and the organic phase was washed two times with 15 mL of H_2O and transferred to a rotary evaporator to evaporate ethyl acetate under low pressure at 35 °C. The residual transparent oil (consisting of DX and residual impurities) was then washed with n-hexane to extract DX. Afterward, n-hexane was evaporated under reduced pressure, and DX was isolated. Then the purified product was dissolved once more in n-hexane to obtain the mixtures used in the reactions (10, 20, and 30 wt% DX in n-hexane). The solution was kept at 5 °C to avoid n-hexane evaporation and DX degradation. The purity of the DX was verified after each batch synthesis through the analysis by paper chromatography and GCMS.

2.4. Catalytic cracking

The tests were carried out in a fixed-bed catalytic cracking unit under atmospheric pressure, as presented in Fig. S1, Supplementary Information. 500 mg of catalyst was put into a quartz tubular reactor and dried under a nitrogen flow of 100 mL min^{-1} at 500 °C for 1 h. After the reactor reached the desired temperature, reactants (pure n-hexane or mixed with 10 to 30 wt% DX) was fed into the reactor of 0.2 mL.min^{-1}. The reaction temperatures used was 500 °C.

The reaction products were distributed as gas, liquid, and coke. The liquid and gas fractions were collected during the whole time of the reaction (total of 15 min). The coke was measured in the spent catalyst. Hence, these fractions were the overall result of this period. The gaseous reaction products were analyzed with a gas chromatograph (Agilent Technologies Micro GC 490) with a TCD detector, and the liquid reaction products were analyzed with a gas chromatograph (Agilent Technologies 7890A CG coupled to a 5975C MS electron impact mode) with an HP-5MS column and a FID detector. The yields of the products were calculated based on the carbon numbers and chromatographic factors, as listed in Table S1, Supplementary Information. The calculations performed to demonstrate the effects obtained from the experiments: conversion, weight hour space velocity (WSHV) and yields of products are based on Eqs. S1-S4 illustrated in the Supplementary Information.

The coke amount was calculated by thermogravimetric analysis of the spent catalyst, (TGA/DTA) (Fig. S5, Supplementary Information). The weight loss from 250 °C to 700 °C in each TG profile was defined as the content of coke in the spent catalyst samples.

3. Results and discussion

3.1. Characterization of zeolites

The physical-chemical properties of fresh and modified Beta, ZSM-5, and USY zeolites are presented in Table 2. A slight reduction in the BET area and volume of micropores was observed after the hydrothermal treatment. This fact may be related to partial blockage of the pores and/or collapse of part of the microporous structure. The SiO_2/Al_2O_3 framework molar ratio increased from HBEA to DHBEA720, as measured by ^{29}Si MAS-NMR.

XRD was used to identify the crystalline phase and also to monitor the loss of crystallinity of the catalyst. The position and intensity of the reflections were compared with data supplied by JCPDS (Joint Committee on Powder Diffraction Standards) reference cards through the International Center for Diffraction Data (ICDD) library. The material phases were identified, with Beta zeolite (BEA) (ICDD 048–0038) being the only phase present in the samples HBEA, DHBEA600, DHBEA720, and DHBEA800. However, partial amorphization of the zeolite structure occurred, reducing the material's crystallinity. A larger crystallinity loss occurred with more severe hydrothermal treatment, as observed in reflections (101) and (116), Fig. 1(a), for example. Therefore, the treatment destroyed the structure of the zeolite at 800 °C, DHBEA800. For this reason, the other characterizations were not carried out with this sample.

The local structure of aluminum atoms was characterized by ^{27}Al MAS-NMR. The NMR spectra of HBEA, DHBEA600 and DHBEA720 samples are shown in Fig. 1 (b), and their relative areas are given in Table S2, Supplementary Information. The identified regions are related to the Al^{IV}, Al^{IV} distorted and/or Al^{V} and Al^{VI} sites [20]. All three samples showed non-structural Al^{VI} (signal in the region between 2 and 1 ppm) and the signals corresponding to Al^{IV} sites (structural) around 55 ppm, characteristic of zeolites. A third signal, in the intermediate region (between 40 and 15 ppm), which may correspond to distorted Al^{IV} sites [24] or to non-structural Al^{V} sites, was also observed in the three samples evaluated.

Hence, the heat treatment reduced the number of tetrahedral sites in the samples, from 55% in HBEA to 40% in HBEA720, Table S2, Supplementary Information. Correspondingly, some aluminum peaks attributed to the Al^{V}, and Al^{VI} were found, indicating that the calcination led to conversion of the tetrahedral aluminum from the lattice to extra lattice. These data can be associated with the reduction in the density of the Brønsted sites (Al^{IV}-OH-Si) present in the zeolites.

The short-range interaction of the silicon atoms was characterized by means of ^{29}Si MAS-NMR. The NMR spectra of the non-calcined and calcined samples are presented in Fig. 1(c) and the data referring to the

Table 2
Textural and structural properties of catalysts employed.

Catalyst	S_{BET} [a] (m^2g^{-1})	$S_{ext.}$ [b] (m^2g^{-1})	$S_{micro.}$ [b] (m^2g^{-1})	$V_{micro.}$ [b] (cm^3g^{-1})	$V_{pore.}$ [c] (cm^3g^{-1})	% Crystallinity XRD[d]	SAR[e] NMR	SAR XRF	Ref.
HBEA	609	182	427	0.18	0.36	100	28	25	This work
DHBEA600	405	143	262	0.11	0.39	98	30	24	
DHBEA720	391	132	259	0.10	0.40	81	43	23	
DHBEA800	333	167	166	0.08	0.48	56	82	22	
ZSM-5	396	101	295	0.12	–	100	18	–	[2,16]
HUSY	627	67	560	0.26	–	–	13	–	[2,16]

[a] BET area (BET method).
[b] External surface area, micropore area and micropore volume (T-plot method).
[c] Total pore volume determined from the adsorbed volume at p/p0 = 0.9.
[d] Normalized using HBEA as 100% and ZSM-5 as reported by the manufacturer.
[e] Framework SiO_2/Al_2O_3 molar ratio by ^{29}Si MAS-NMR for Beta.

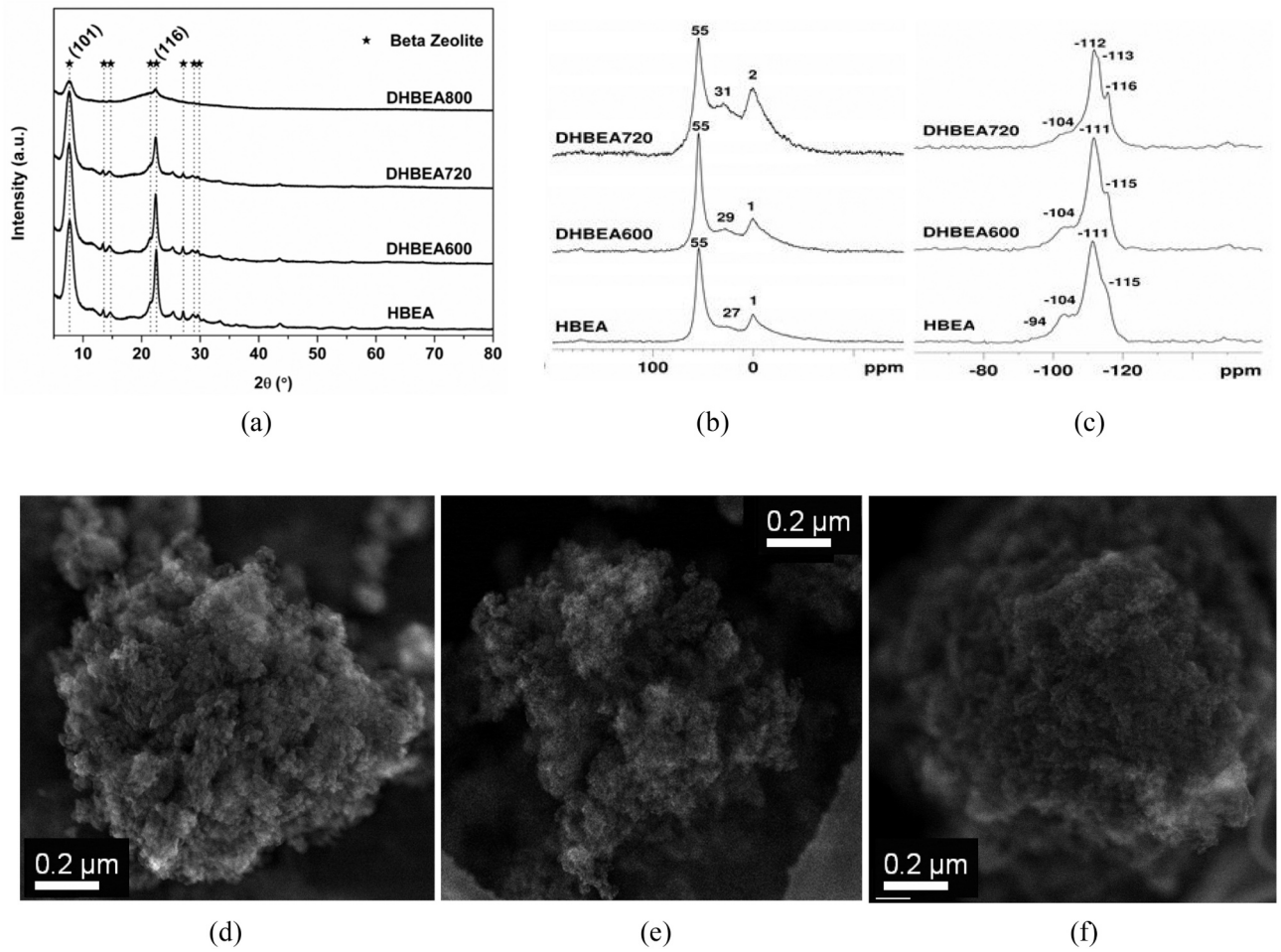

Fig. 1. Characterization of Beta catalysts: (a) XRD, (b) ^{27}Al MAS-NMR, (c)^{29}Si MAS-NMR, (d) SEM of HBEA, (e) SEM of DHBEA600, and (f) SEM of DHBEA720.

signal areas, in Table S3, Supplementary Information. Typically, there were at least 4 signals, corresponding to the species Si(0Al), Si(1Al) and Si(2Al), around −116/111, −104 and − 98 ppm respectively. The steam heat treatment caused a reduction in the percentage of Si(2Al) sites, while the Si(0Al) signals markedly increased. A decrease in the area of Si-O-Al type sites was observed as a function of the sample analyzed: HBEA > BEADH600 > BEADH720. The SAR results measured from the ^{29}Si MAS-NMR spectra were consistent with this trend, although the absolute values may be underestimated due to the overlap of Si(1Al) sites with SiOH-type sites. The sample DHBEA720 showed the highest SiO_2/Al_2O_3 (SAR) ratio. Therefore, the results of ^{27}Al MAS-NMR and ^{29}Si MAS-NMR were consistent.

In addition, SEM microscopy, Fig. 1(d), (e), (f), produced similar images of HBEA, DHBEA600, and DHBEA720. The same results was showed in the TEM microscopy (Fig. S2 in the SI). Therefore, the hydrothermal deactivation did not severely affect the zeolite crystal shape and size of the remaining crystalline phase, as also observed in the XRD results.

Table 3 shows the Lewis and Brønsted acid sites for fresh and modified catalysts, measured by pyridine adsorption. There were more Lewis acid sites than Brønsted sites. For example, for HBEA, the B/L ratio was 0.75. However, when the catalyst was subjected to hydrothermal deactivation, both sites decreased, probably due to the partial structural collapse during steam treatment. The B/L ratio was further reduced. In addition, steaming caused an increase in the intensity of the SI-OH IR band and decreased the total number of acid sites, as presented in Fig. 2, in accordance with the assignments of Marques et al. [25].

Table 3
Acid site characterization (by FTIR of pyridine) of fresh and deactivated HBEA.

Catalyst	Brønsted[a] (μmol/g)	Lewis[a] (μmol/g)	Total acid sites (μmol/g)	B/L ratio
HBEA	197	261	459	0.75
DHBEA600	64	90	154	0.71
DHBEA720	36	74	110	0.48

[a] Concentration of the respective sites retained at 150 °C.

3.2. A brief comparison between different zeolites: Beta, USY and ZSM-5

The cracking of fresh Beta was compared with those previously published using zeolites HUSY and HZSM-5 for cracking DX in a fixed-bed reactor [2,16]. Table 4 summarizes the results of three types of catalysts using the same experimental conditions: 10 wt% DX in n-hexane mixture and 400 mg of catalyst (WHSV 20 h^{-1}) at 500 °C. The liquid product is the total liquid collected, including the unreacted n-hexane. Hence, the values of Beta in Table 4 are the sum of liquid products and unreacted n-hexane.

Among the zeolites studied, HZSM-5 produced the highest conversion of n-hexane, but DX was not fully converted. On the other hand, HBEA produced the lowest conversion of n-hexane, with 100% conversion of DX. HZSM-5 yielded the largest fraction of gaseous products and the lowest fraction of coke.

Hence, HZSM-5 zeolite exhibited characteristics as in the cracking of hydrocarbons. Due to the small pore size and high acidity of HZSM-5 zeolite, it has facility to crack hydrocarbons into fractions with light molecular weight while inhibiting coke precursors from combining to

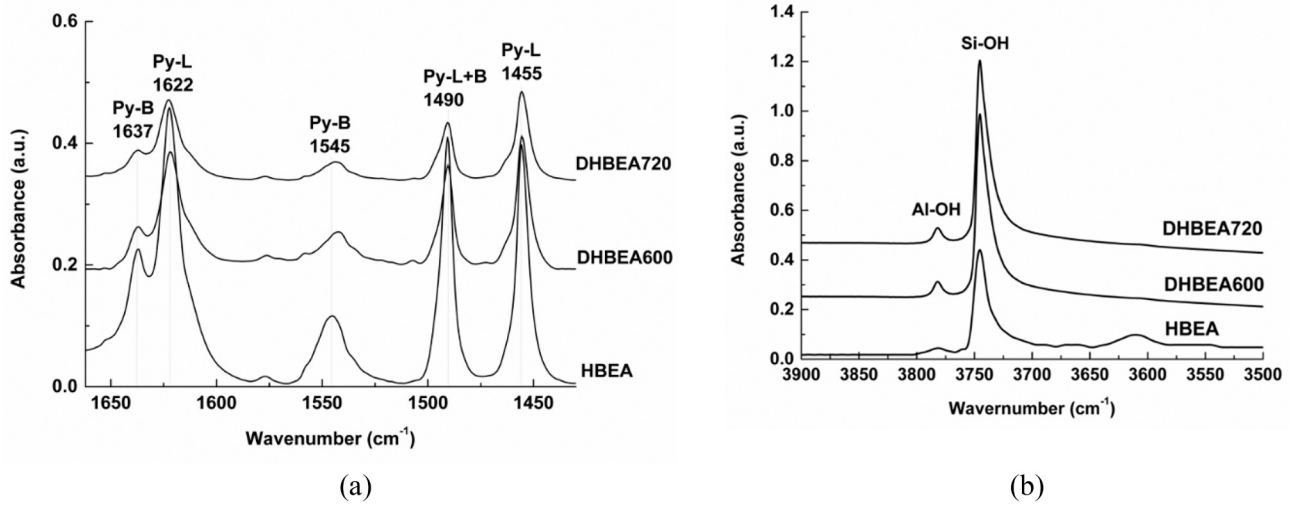

Fig. 2. Characterization of Beta catalysts: FTIR spectra obtained from adsorbed pyridine (a) acid sites, (b) bridging hydroxyl. Legend: Py = Pyridine; B = Brønsted site; L = Lewis site and B + L = overlapping of peaks attributed to Lewis and Brønsted sites.

Table 4
Conversion and yields of liquid, gas, coke, unreacted n-hexane, and water obtained by catalytic cracking of pure n-hexane and 10% DX/ n-hexane in HZSM-5[a], HBEAa and HUSY[a].

Catalyst (SAR)	Feed	Gas (wt%)	Liquid (wt%)	Coke (wt%)	Conversion (%)		Ref.
					nC_6	DX	
HZSM-5	nC_6	55.6	44.2	0.2	71	–	[2,16]
(18)	DX/ nC_6	29.1	70.5	0.4	43	94	
HBEA	nC_6	19.0	80.5	0.5	40	–	This work
(28)	DX/ nC_6	14.0	84.2	1.8	20	100	
HUSY	nC_6	26.5	71.1	2.4	41	–	[2,16]
(13)	DX/ nC_6	24.4	71.0	4.6	30	100	

[a] 400 mg zeolite - WHSV ($20h^{-1}$), 500 °C reaction temperature and normalized to 100% mass balance.

generate coke. However, the small pore size also limits the accessibility of larger DX molecules to the active sites. Hence, the conversion of DX was lower than the other zeolites.

HUSY zeolite effectively transformed DX into valuable products, Table 4. However, it also produced the highest coke yield. The high activity can be attributed to the high number of acid sites due to the SAR value, 13, of the zeolite used. The high coke yield could be due to the large pore volume and high hydrogen transfer capacity. The amount of coke can be reduced by hydrothermal treatment of Y zeolites, reducing the number of acid sites. A reduction of coke 15 wt% to 8 wt% was observed with steam-treated USY when compared to fresh USY in the mixture of 30% DX / n-hexane [2]. Nonetheless, compared to fresh Beta zeolite, HUSY produced a coke yield greater than 50% under the same test conditions.

In short, HBEA zeolite efficiently converted sugar acetals. The hydrocarbon liquid product was the highest, the gaseous product was the lowest, and the coke showed an intermediate value between the HUSY and HZSM-5 zeolites. Possibly its intermediate pore size between HZSM-5 and HUSY is an important factor in minimizing the interference of n-hexane cracking.

3.3. Optimization of the acidic properties of Beta by hydrothermal deactivation for DX conversion

3.3.1. Effect of hydrothermal treatment temperature

The effect of hydrothermal treatment at temperatures of 600 °C (DHBEA600), 720 °C (DHBEA720) and 800 °C (DHBEA800) are summarized in Table 5. The conversion of n-hexane decreased ~3-fold with increasing deactivation temperature from 600 °C to 800 °C. In the presence of 10 wt% DX, the conversion of n-hexane decreased even more. The sample after treatment with 800°C showed only 7.3% conversion of n-hexane. This result can be attributed to deterioration of the structure with increasing steaming temperature, as illustrated in the diffractogram in Fig. 1(a), and also in the ^{29}Si and ^{27}Al MAS-NMR spectra (Fig. S6, Supplementary Information). DX continued to be 100% converted even when the number of Beta acid sites decreased due to the hydrothermal treatment. These results are in accordance with the objective of this work: to reduce the number of active sites to reduce the participation of n-hexane in the products and increase the ratio between the liquid product yield over the gaseous product yield, as presented in Fig. 3.

Focusing on the results on the conversion of DX/n-hexane mixture, even with the decrease of these sites, the DX is completely converted. The conversion of n-hexane showed an increase with the increase on the amount of acidic sites and with the addition of DX in the mixture this characteristic becomes more evident, as shown in Fig. 4(a), confirming DX's preference for zeolite sites. In Fig. 4(b), the increase in n-hexane conversion could be the main factor that increased the yield of the gas, but did not affect significantly the coke yield, Fig. S7 (Supplementary Information).

The formation of aromatics also decreased with the increase of deactivation temperature. As aromatics are probably formed from hydrogen transfer reactions, this decrease may be interpreted mainly due to the decrease in acid site density.

However, the effect of acidity of the overall transformation is complex. It is very likely that changes in acidic sites on the catalysts change their interaction not only with the reactants, but also with the intermediate products formed. Further, steam deactivation could also change the amount and type of non-framework alumina. This in turn may limit or block reagent access and product desorption from active sites.

With respect to the DX/n-hexane mixture, the n-hexane conversion decreased 2-fold or more compared to the case of pure n-hexane. The coke yield also decreased with increased deactivation. Finally, the liquid product increased ~15 wt% while the gas products decreased ~25 wt% comparing the yields from deactivated Beta at 800 °C with that from

Table 5
Conversion and yields of liquid, gas, coke, unreacted n-hexane, and water obtained by catalytic cracking of pure n-hexane and 10% DX/ n-hexane in Beta [a] zeolites hydrothermally treated at different temperatures.

Deactivation temperature (°C)	10% DX / n-hexane				n-hexane			
	0[b]	600	720	800	0[b]	600	720	800
Conversions (%)								
n-hexane Conversion	22.9	24.1	19.2	7.3	41.5	34.6	24.1	14.1
DX Conversion	100	100	100	100	–	–	–	–
Yield (wt%)								
Gas	16.2	10.8	8.1	4.1	24.1	25.5	14.5	4.9
Liquid	82.0	87.8	90.7	94.5	75.3	74.1	85.3	95.0
Liquid Products[c]	10.7	17.6	15.4	8.2	16.8	8.7	9.4	9.0
Oxygenates	0.5	0.4	1.0	1.1	–	–	–	–
n-Hexane	69.4	68.3	72.7	83.4	58.5	65.4	75.9	86.0
Water[d]	1.4	1.5	1.6	1.8	–	–	–	–
Coke	1.8	1.5	1.3	1.4	0.5	0.4	0.2	0.1

[a] 500 mg zeolite - WHSV (16 h^{-1}) and 500 °C.
[b] Fresh Beta.
[c] Total liquid products considering the following: paraffins, olefins, monoaromatics, polyaromatics, unidentified products.
[d] Data from oxygen balance.

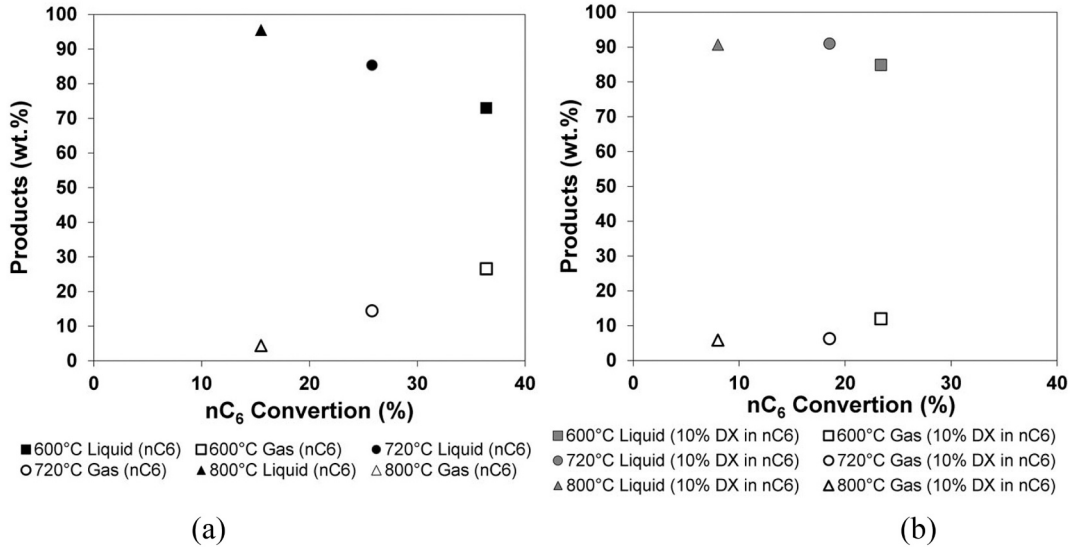

Fig. 3. Liquid and gas yields and n-hexane conversion obtained by catalytic cracking of pure n-hexane and 10% DX/ n-hexane in Beta zeolites hydrothermally treated at different temperatures with 500 mg of zeolite (WHSV 16 h^{-1}) at 500 °C. Error of experiments (1% - 3% of the gas and liquid yield value) are reported in (Table S4, supplementary information). Legend: (a) - Pure n-hexane; (b) - 10% DX in n-hexane.

fresh Beta.

For deoxygenation, the water fraction remained similar to that of fresh Beta, indicating that the deoxygenation via dehydration was still very important and independent of acid sites (density and type). However, the main products in the organic liquid phase were monoaromatics. The classes of hydrocarbons are described in Fig. S3, Supplementary Information, with aromatic yields of 8 to 12 carbons for pure n-hexane and the mixture of Dx/n-hexane. The amount of oxygenates increased with increasing severity of deactivation, Fig. 5(b). Thus, the catalyst acid properties (density and probably type of acid sites) influenced the deoxygenation reactions. For example, the CO/CO_2 ratio, Table S5, Supplementary Information was maximized with Brønsted acid sites. This is probably related to the type of oxygenates in function of increasing reaction time. In summary, hydrothermal deactivation of Beta zeolite changed in the expected direction, consistent with the results of the deactivation of USY: decreased coke and gas yields.

3.3.2. *Effect of DX percent on hydrothermally treated DHBEA720*

The effect was analyzed of variation of the concentration of DX (10%, 20% and 30% by weight) in the catalyst with intermediate hydrothermal treatment (720 °C).

Table 6 shows that the conversion and the gas fraction decreased, while the coke fraction increased with rising DX % in the mixture with both DHBEA720 and HBEA. The liquid fraction increased slightly, and this liquid fraction from DHBEA720 was much greater than that obtained by HBEA.

We would draw special attention to the cracking of up to 20%DX in n-hexane with DHBEA720. Even with fewer active sites, DX was fully converted. Hydrocarbons were the main products and oxygenates were only ~1%. The classes of hydrocarbons are described in Fig. 6(b). However, when the mixture contained more DX, as in the case of the 30 wt% DX mixture, the conversion to hydrocarbons was no longer satisfactory. The amount of oxygenates sharply increased from 0.9 to 5.4%. The effect of increasing DX % in the feed mixture on the distribution of the liquid products is illustrated by Fig. 6(a).

Indeed, the high conversion of DX indicated that the initial decomposition of DX does not require a large number of acid sites or high-strength sites. However, further transformation of the oxygenated intermediate products may require such sites. The oxygenates are mainly

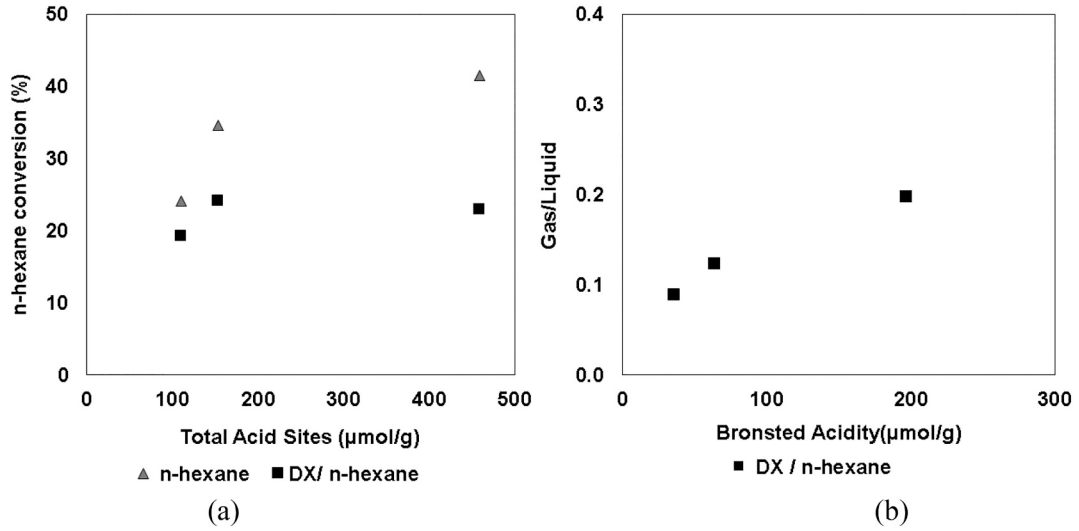

Fig. 4. Relationship between (a) n-hexane conversion and total acid sites; (b) gas yield and Bronsted acidity of the HBEA, DHBEA600 and DHBEA720 catalysts.

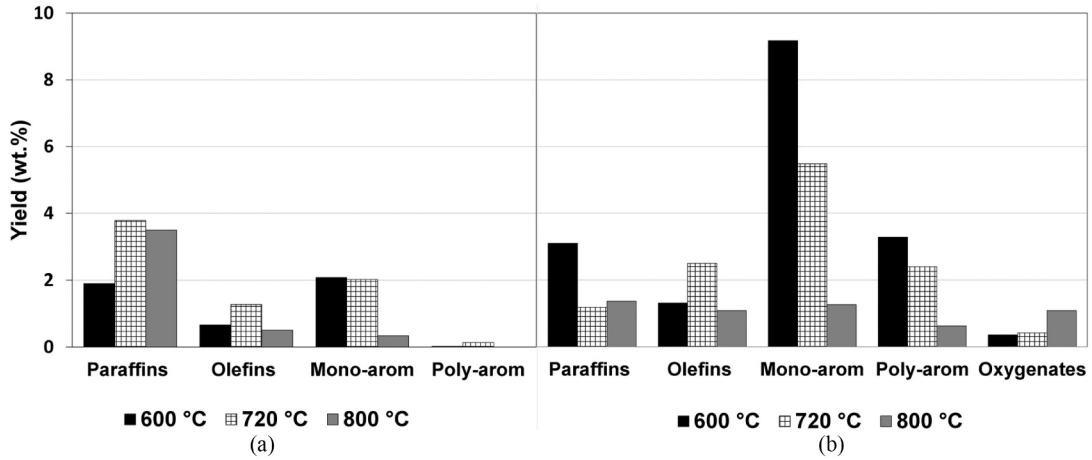

Fig. 5. Yields of liquid products obtained by catalytic cracking of pure n-hexane and 10% DX/ n-hexane in Beta zeolites hydrothermally treated at different temperatures with 500 mg of zeolite (WHSV 16 h^{-1}) at 500 °C. Legend: (a) - Pure n-hexane; (b) - 10% DX in n-hexane; Mono-arom – monoaromatics; Poly-arom – polyaromatics.

Table 6
Conversion and yields of liquid, gas, coke, unreacted n-hexane, and water obtained by catalytic cracking with 10%, 20% and 30% of DX/ n-hexane in HBEA[a] and DHBEA720[a].

DX content (wt%)	DHBEA720			HBEA	
	10	20	30	10	30
Conversions (%)					
n-hexane Conversion	19.2	3.1	2.2	22.9	5.7
DX Conversion	100	100	99.8	100	99.6
Yields (wt%)					
Gas	8.1	6.6	6.0	16.2	12.8
Liquid	90.7	91.7	91.2	82.0	84.3
Liquid Products[b]	15.4	8.8	9.8	10.7	11.2
Oxygenates	1.0	0.9	5.4	0.5	2.0
n-Hexane	72.7	77.6	68.5	69.4	66.0
Water[c]	1.6	4.4	7.5	1.4	5.1
Coke	1.3	1.7	2.9	1.8	3.1

[a] 500 mg zeolite - WHSV (16 h^{-1}) and 500 °C reaction temperature.
[b] Total liquid products considering the following: paraffins, olefins, monoaromatics, polyaromatics, unidentified products, and unreacted DX (30%).
[c] Data from oxygen balance.

ketones, furans and alkyl-furans, which can be used as gasoline octane boosters [26]. The largest amount of oxygenates from the 30 wt% DX mixture were ketones. However, they were much smaller in amount than in the other mixtures. Furans were observed in significant concentrations in all tests. Phenols and alkyl-phenols were observed in lower concentrations. The details are given in Table S6, Supplementary Information.

As previously observed, water is an important deoxygenated product of deoxygenation. The results in Table 6 show clearly that the water yield was proportional to the amount of DX in the mixture also illustrated in Fig. S4, Supplementary Information. Thus, DX is primarily deoxygenated, yielding water, without much carbon loss overall.

Table 7 shows that the CO/CO_2 ratio increased with DX wt% also presented in Fig. S4, Supplementary Information. From literature reports, we expected larger amounts of ketones to be deoxygenated, producing a higher CO/CO_2 ratio [27]. In contrast, acetone produced more CO_2 than CO [28]. Thus, most probably the type of oxygenates will affect the relative importance of decarbonylation and decarboxylation reactions.

To guide our discussion on the role of the zeolites and their modifications, we would describe the major reactions that the model molecule DX undergoes on the acidic zeolite based on the intermediates

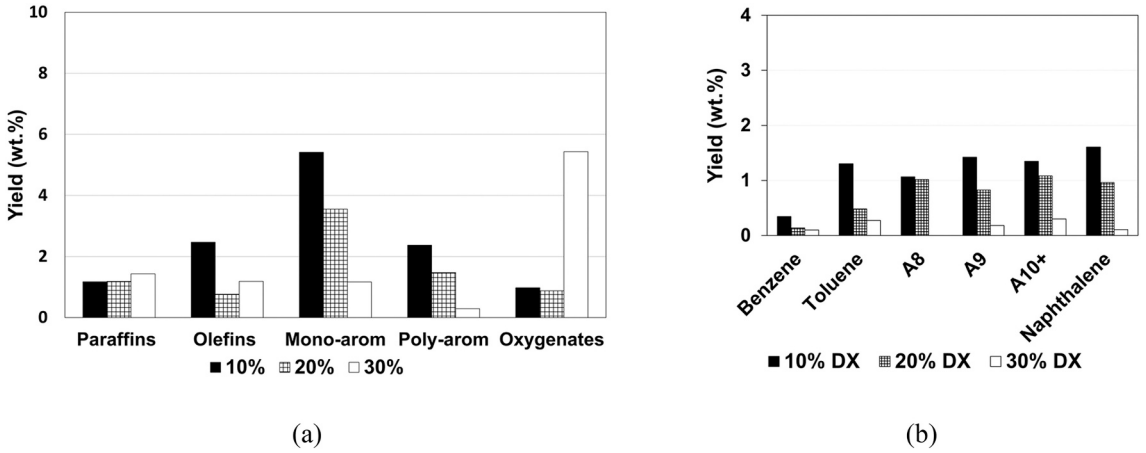

Fig. 6. Yields of liquid fraction obtained by catalytic cracking with percentage variation of 10%, 20% and 30% of DX/ n-hexane of DHBEA720 at 500 mg zeolite (WHSV 16 h^{-1}) at 500 °C. Legend: (a) liquid product; (b) the classes of hydrocarbons; Mono-arom – monoaromatics; Poly-arom – polyaromatics; A8 - aromatics with 8 carbons; A9 - aromatics with 9 carbons; A10+ – aromatics of 10 to 12 carbons.

Table 7
Yields of gas obtained by catalytic cracking with percentage variation of 10%, 20%, and 30% of DX/ n-hexane in HBEA[a] and DHBEA720[a].

Gas (wt%)												
	DX (%)	H_2	CH_4	C_2H_4	C_2H_6	C_3H_8	C_3H_6	C_4H_{10}	C_4H_8	CO	CO_2	Total
DHBEA720	10	0.2	2.6	0.5	0.2	0.3	1.1	0.1	0.3	1.8	0.9	8.1
	20	0.1	1.9	0.2	0.1	0.0	0.3	0.0	0.0	2.9	1.1	6.6
	30	0.1	2.1	0.2	0.0	0.0	0.1	0.0	0.0	2.9	0.6	6.0
HBEA	10	0.4	0.8	1.1	0.3	4.2	4.2	1.0	0.9	1.8	1.4	16.2
	30	0.2	2.3	0.4	0.1	0.2	0.7	0.3	0.3	6.1	2.1	12.8

[a] 500 mg zeolite - WHSV (16 h^{-1}) and 500 °C reaction temperature.

determined in this and previous works and also on the change of products distribution as a function the advance in the transformation due to increase severity of the experiments. The key reactions that marked the final products observed are underlined. A proposed reaction pathway is shown in Fig. 7.

The parent molecules first decompose partially loosing water (main products at low DX conversion), acetone and some furans derivatives. So the first group of reactions are rearrangement and dehydration reactions [29]. These rather high molecular weight intermediates further break up into smaller oxygenates, such as ketones and furans.

Hydrocarbons are formed when these oxygenates undergoes decarbonylation [30] and decarboxylation [31]. We observed CO and CO_2 in the gas phase. Some light hydrocarbons are formed just by cracking or dealkylation of the larger hydrocarbon molecules.

The olefins formed from cracking undergo oligomerization, and aromatization [32,33], thus both naphthene and aromatics are formed. (The Diels elder reactions are considered as an oligomerization).

In spite of the above main types of reactions, we could not rule out other types of reactions such as: aromatization directly by ketone molecules, acid catalysed condensation between ketones, between ketones and furan derivatives, between furan derivatives with olefins [34,35]. All these reaction will further produce water and affect the hydrocarbon distribution. Yet, if we keep the hypothesis that dehydrations, decarbonylation/decarboxylation and oligomerization/aromatization as the three main types of reactions, we can interpret the demands of the catalytic sites and our results as follows:

The dehydrations require only mild acid sites and hence we observed DX was almost all transformed with the most deactivated beta catalyst.

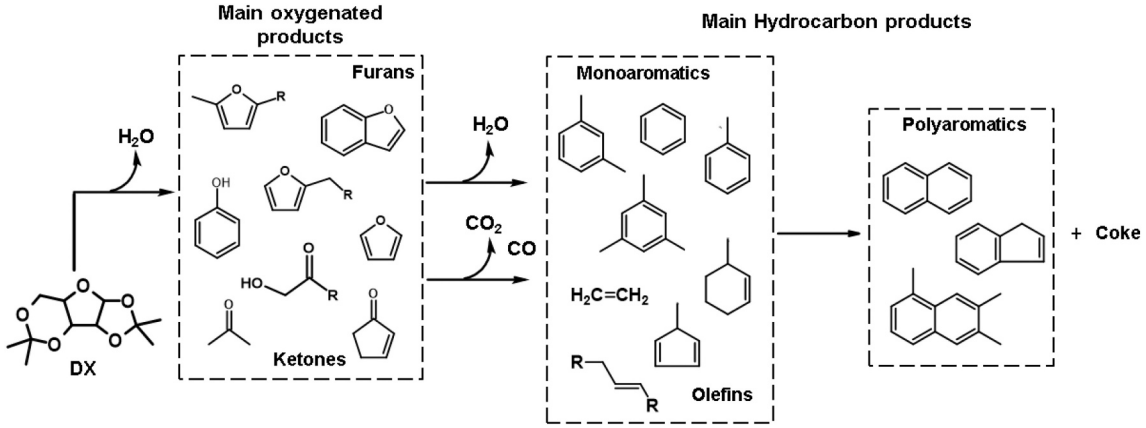

Fig. 7. Proposal of a reactional pathway for the catalytic cracking of DX-derived oxygenates.

The decarbonylation and decarboxylation occurs when the degree of transformation is more advanced, competing with other reactions as oligomerization /aromatization and C—C bond cracking for the stronger acid sites. Hence we need more active sites to remove all oxygenates in the products.

It preferable that aromatization take place more than the other competing reactions cited since this gives more desired liquid products.

DX further reduced the conversion of n-hexane due to competition for active sites, reducing the gas generated by the cracking of n-hexane. A clear indication was from the drastic decrease in C_3 and C_4 products. In contrast, a higher yield of methane was observed in the deactivated Beta. In the test with 20% DX, methane yield was 1.9% with only a yield of C_3 and undetectable C_4, as presented, Table 7. This should be interpreted as the effect of type of acid sites in deactivation catalysts, since deactivation decreases the number of Brønsted sites, and thus the protolytic reactions [25].

To sum up, the successful transformation of higher DX % (up to 20%) by steam deactivated Beta improving the liquid yield over gas yield, with acceptable coke and oxygenated intermediates reinforced the advantage using less acidic catalysts. However. further increase in concentration of DX did not result in complete conversion into hydrocarbon products in the fixed-bed unit with this catalyst. The potential of the less acidic catalyst could probably be explored in other reactor configurations that allow for a much higher catalyst-to-feed ratio.

4. Conclusions

The conversion of sugar acetals to bio-hydrocarbons in the presence of hydrothermally deactivated Beta zeolite was studied using a fixed-bed reactor. Comparing the tests with 10% DX in n-hexane of fresh zeolites (Beta, ZSM-5, and USY) under the same reaction conditions, we observed that Beta had greater activity, higher yield of liquid products and less interference of the cracking of n-hexane. Beta gave an intermediate gas and coke yield between ZSM-5 and USY. This could be due to its intermediate pore structure and acidity.

Reducing the number of acid sites of Beta by hydrothermal deactivation resulted in lower gas formation, while still obtaining full DX conversion without increasing coke in mixtures up to 20 wt% DX. However, the intermediate oxygenates were not converted to hydrocarbons readily.

We believe that to make better use of Beta zeolite, for example, in the reduction of n-hexane interference and in the conversion of 100% DX into higher value-added products in processes with higher DX concentrations. Beta should be applied in a reactor configuration that can provide a greater number of acid sites with lower strength.

Credit authorship contribution statement

Cristiane Cardoso carried out all experiments, prepare Figures and write the manuscript, Rosane A. S. San Gil characterized catalysts by NMR, Jeroen A. Van Bokhoven helped in characterized catalysts, Yiu Lau Lam and Marcelo Maciel Pereira conduct the research.

Declaration of Competing Interest

The authors declare the following financial interests/personal relationships which may be considered as potential competing interests:

Marcelo Maciel Pereira, on behalf of all authors, declare that there are no competing financial interests or personal relationships that could have appeared to influence the work reported in this paper.

Data availability

Data will be made available on request.

Acknowledgments

This work was supported CAPES (Coordenação de aperfeiçoamento de pessoal de nível superior), process 88881.189032/2018-01, granting a sandwich scholarship, and FAPERJ (Fundação Carlos Chagas Filho de Amparo à Pesquisa do Estado do Rio de Janeiro) (contracts 210.068/2020 and E-26/210.799/2021).

Appendix A. Supplementary data

Supplementary data to this article can be found online at https://doi.org/10.1016/j.catcom.2022.106519.

References

[1] D.N. Dos Santos, I.V. Pedrosa, C.R.R. Fernandes, A. Lachgar, M. Neli, R. Garrett, Y. L. Lam, M.M. Pereira, Catalytic sugarcane bagasse transformation into a suitable biocrude for hydrocarbon production in typical refinery processes, Sustain. Energy Fuel 4 (2020) 4158–4169, https://doi.org/10.1039/d0se00220h.

[2] J. Pinto, I. Pedrosa, C. Linhares, R.A.S. San Gil, Y.L. Lam, M.M. Pereira, Ketal sugar conversion into green hydrocarbons by Faujasite zeolite in a typical catalytic cracking process, Front. Chem. 7 (2019) 1–14, https://doi.org/10.3389/fchem.2019.00720.

[3] M.A. Den Hollander, M. Wissink, M. Makkee, J.A. Moulijn, Gasoline conversion: reactivity towards cracking with equilibrated FCC and ZSM-5 catalysts, Appl. Catal. A Gen. 223 (2002) 85–102, https://doi.org/10.1016/S0926-860X(01)00745-1.

[4] A.D.R. Pinho, M.B.B. De Almeida, F.L. Mendes, V.L. Ximenes, L.C. Casavechia, Co-processing raw bio-oil and gasoil in an FCC unit, Fuel Process. Technol. 131 (2015) 159–166, https://doi.org/10.1016/j.fuproc.2014.11.008.

[5] Á. Ibarra, A. Veloso, J. Bilbao, J.M. Arandes, P. Castaño, Dual coke deactivation pathways during the catalytic cracking of raw bio-oil and vacuum gasoil in FCC conditions, Appl. Catal. B Environ. 182 (2016) 336–346, https://doi.org/10.1016/j.apcatb.2015.09.044.

[6] S. van Dyk, J. Su, J.D. Mcmillan, J. John Saddler, Potential synergies of drop-in biofuel production with further co-processing at oil refineries, Biofuels Bioprod. Biorefin. 13 (2019) 760–775, https://doi.org/10.1002/bbb.1974.

[7] N. Batalha, A.V. Da Silva, M.O. De Souza, B.M.C. Da Costa, E.S. Gomes, T.C. Silva, T.G. Barros, M.L.A. Gonçalves, E.B. Caramão, L.R.M. Dos Santos, M.B.B. Almeida, R.O.M.A. De Souza, Y.L. Lam, N.M.F. Carvalho, L.S.M. Miranda, M.M. Pereira, Gasoline from biomass through refinery-friendly carbohydrate-based bio-oil produced by ketalization, ChemSusChem. 7 (2014) 1627–1636, https://doi.org/10.1002/cssc.201301242.

[8] A.P. Pinheiro Pires, J. Arauzo, I. Fonts, M.E. Domine, A. Fernández Arroyo, M. E. Garcia-Perez, J. Montoya, F. Chejne, P. Pfromm, M. Garcia-Perez, Challenges and Opportunities for Bio-Oil Refining: A Review, 2019, https://doi.org/10.1021/acs.energyfuels.9b00039.

[9] D.A. Bulushev, J.R.H. Ross, Catalysis for conversion of biomass to fuels via pyrolysis and gasification: a review, Catal. Today 171 (2011) 1–13, https://doi.org/10.1016/j.cattod.2011.02.005.

[10] G. Lyu, S. Wu, H. Zhang, Estimation and comparison of bio-oil components from different pyrolysis conditions, Front. Energy Res. 3 (2015) 1–11, https://doi.org/10.3389/fenrg.2015.00028.

[11] I.A. Vasalos, A.A. Lappas, E.P. Kopalidou, K.G. Kalogiannis, Biomass catalytic pyrolysis: process design and economic analysis, Wiley Interdiscip. Rev. Energy Environ. 5 (2016) 370–383, https://doi.org/10.1002/wene.192.

[12] W. Jin, L. Pastor-Pérez, J. Yu, J.A. Odriozola, S. Gu, T.R. Reina, Cost-effective routes for catalytic biomass upgrading, Curr. Opin. Green Sustain. Chem. 23 (2020) 1–9, https://doi.org/10.1016/j.cogsc.2019.12.008.

[13] L. Sauvanaud, Y. Mathieu, A. Corma, L. Humphreys, W. Rowlands, T. Maschmeyer, Co-processing of lignocellulosic biocrude with petroleum gas oils, Appl. Catal. A Gen. 551 (2018) 139–145, https://doi.org/10.1016/j.apcata.2017.09.029.

[14] R. Garrett, T.G. Barros, M.O. De Souza, B.M.C. Da Costa, M.M. Pereira, L.S. M. Miranda, Unveiling the chemical composition of sugar cane biocrudes by liquid chromatography-tandem mass spectrometry, Energy Fuel 29 (2015) 8082–8087, https://doi.org/10.1021/acs.energyfuels.5b02317.

[15] G. Jiménez-García, R. Maya-Yescas, Differences between fisher-Tropsch synthesis of either gasoline or diesel based on changes of entropy and free energy, Fuel. 149 (2015) 184–190, https://doi.org/10.1016/j.fuel.2014.08.041.

[16] N. Batalha, J. Pinto, H. Ferreira, D.C. Baptista, L.S.M. Miranda, M.M. Pereira, Biohydrocarbons production under standard refinery conditions by means of a representative ketal compound of biocrude, Energy Technol. 5 (2017) 428–441, https://doi.org/10.1002/ente.201600313.

[17] A. Aitani, T. Yoshikawa, T. Ino, Maximization of FCC light olefins by high severity operation and ZSM-5 addition, Catal. Today 60 (2000) 111–117, https://doi.org/10.1016/S0920-5861(00)00322-9.

[18] M.A. Bari Siddiqui, A.M. Aitani, M.R. Saeed, S. Al-Khattaf, Enhancing the production of light olefins by catalytic cracking of FCC naphtha over mesoporous ZSM-5 catalyst, Top. Catal. 53 (2010) 1387–1393, https://doi.org/10.1007/s11244-010-9598-1.

[19] A. Fúnez, A. De Lucas, P. Sánchez, M.J. Ramos, J.L. Valverde, Hydroisomerization in liquid phase of a refinery naphtha stream over Pt-Ni/H-beta zeolite catalysts, Chem. Eng. J. 136 (2008) 267–275, https://doi.org/10.1016/j.cej.2007.03.062.

[20] J. Dědeček, E. Tabor, S. Sklenak, Tuning the aluminum distribution in zeolites to increase their performance in acid-catalyzed reactions, ChemSusChem. 12 (2019) 556–576, https://doi.org/10.1002/cssc.201801959.
[21] P. Castaño, G. Elordi, M. Olazar, A.T. Aguayo, B. Pawelec, J. Bilbao, Insights into the coke deposited on HZSM-5, Hβ and HY zeolites during the cracking of polyethylene, Appl. Catal. B Environ. 104 (2011) 91–100, https://doi.org/10.1016/j.apcatb.2011.02.024.
[22] M. Guisnet, P. Magnoux, Coking and deactivation of zeolites. Influence of the pore structure, Appl. Catal. 54 (1989) 1–27, https://doi.org/10.1016/S0166-9834(00)82350-7.
[23] E.F. Sousa-Aguiar, Y Zeolites as a Major Component of FCC Catalysts: Main Challenges in the Modification Thereof, Elsevier B.V, 2016, https://doi.org/10.1016/B978-0-444-63506-8.00007-0.
[24] S.M. Maier, A. Jentys, J.A. Lercher, Steaming of zeolite BEA and its effect on acidity: a comparative NMR and IR spectroscopic study, J. Phys. Chem. C 115 (2011) 8005–8013, https://doi.org/10.1021/jp108338g.
[25] J.P. Marques, I. Gener, J.M. Lopes, F. Ramôa Ribeiro, M. Guisnet, N-heptane cracking on dealuminated HBEA zeolites, Catal. Today (2005) 726–733, https://doi.org/10.1016/j.cattod.2005.07.003.
[26] J.H. Badia, E. Ramírez, R. Bringué, F. Cunill, J. Delgado, New octane booster molecules for modern gasoline composition, Energy Fuel 35 (2021) 10949–10997, https://doi.org/10.1021/acs.energyfuels.1c00912.
[27] A.G. Gayubo, A.T. Aguayo, A. Atutxa, R. Aguado, J. Bilbao, Transformation of oxygenate components of biomass pyrolysis oil on a HZSM-5 zeolite, I. Alcohols and phenols, Ind. Eng. Chem. Res. 43 (2004) 2610–2618, https://doi.org/10.1021/ie030791o.
[28] T.A. Palankoev, K.I. Dement'Ev, D.V. Kuznetsova, G.N. Bondarenko, A.L. Maximov, Acetone Reaction Pathways as a Model Bio-oxygenate in a Hydrocarbon Medium on Zeolite y and ZSM-5 Catalysts: In Situ FTIR Study, ACS Sustain. Chem. Eng. 8 (2020) 10892–10899, https://doi.org/10.1021/acssuschemeng.0c03215.
[29] G.W. Huber, R.D. Cortright, J.A. Dumesic, Renewable alkanes by aqueous-phase reforming of biomass-derived oxygenates, Angew, Chemie - Int. Ed. 43 (2004) 1549–1551, https://doi.org/10.1002/anie.200353050.
[30] Y.T. Cheng, G.W. Huber, Production of targeted aromatics by using Diels-Alder classes of reactions with furans and olefins over ZSM-5, Green Chem. 14 (2012) 3114–3125, https://doi.org/10.1039/c2gc35767d.
[31] R.H. Venderbosch, A.R. Ardiyanti, J. Wildschut, A. Oasmaa, H.J. Heeres, Stabilization of biomass-derived pyrolysis oils, J. Chem. Technol. Biotechnol. 85 (2010) 674–686, https://doi.org/10.1002/jctb.2354.
[32] J.D. Adjaye, N.N. Bakhshi, Production of hydrocarbons by catalytic upgrading of a fast pyrolysis bio-oil. Part I: conversion over various catalysts, Fuel Process. Technol. 45 (1995) 185–202, https://doi.org/10.1016/0378-3820(95)00040-E.
[33] A. De Lucas, P. Canizares, A. Durán, A. Carrero, Dealumination of HZSM-5 zeolites: effect of steaming on acidity and aromatization activity, Appl. Catal. A Gen. 154 (1997) 221–240, https://doi.org/10.1016/S0926-860X(96)00367-5.
[34] L. Wu, T. Moteki, A.A. Gokhale, D.W. Flaherty, F.D. Toste, Production of fuels and chemicals from biomass: condensation reactions and beyond, Chem. 1 (2016) 32–58, https://doi.org/10.1016/j.chempr.2016.05.002.
[35] H. Shi, Valorization of Biomass-derived Small Oxygenates: Kinetics, Mechanisms and Site Requirements of H 2 -involved Hydrogenation and Deoxygenation Pathways over Heterogeneous Catalysts, 2019, pp. 1–55, https://doi.org/10.1002/cctc.201801828.